ACS OMEGA

http://pubs.acs.org/journal/acsodf

Article

An Electrochemical Sensor for Quantitation of the Oral Health Care Agent Chlorogenic Acid Based on Bimetallic Nanowires with Functionalized Reduced Graphene Oxide Nanohybrids

Wei Li, Xiuli Deng, Ziyu Wu, Louqiang Zhang, and Jian Jiao*

Cite This: *ACS Omega* 2022, 7, 4614–4623

Read Online

ACCESS | Metrics & More | Article Recommendations | Supporting Information

ABSTRACT: Chlorogenic acid (CGA), a phenolic acid from coffee, has been regarded as a powerful ingredient against oxidative stress and inflammation. Meanwhile, its healing feature to interfere with periodontal disease (PD) makes it a promising drug candidate. However, the existing methods for chlorogenic acid detection limit its practical application in purification and further pharmacological study in stomatology due to their lack of accuracy and productivity. Therefore, it is crucial to find a forceful approach to precisely evaluate CGA for an in-depth anti-PD study. In this work, we reported a facile and controllable synthesis of Pt@Pd nanowires (NWs) in a non-compacted core−shell structure with high electrocatalytic activity. In addition, polyethylenimine (PEI)-capped reduced graphene oxide (rGO) nanoflakes provided large binding sites for a network structure composed of interweaved Pt@Pd nanowires and protected hemin from self-destruction, which empowered Pt@Pd NWs-Hemin-PEI-rGO nanohybrids to own a large electroactive surface area and great electrochemical property for CGA detection. The enzyme-free electrochemical sensor based on Pt@Pd NWs-Hemin-PEI-rGO displayed a favorable capacity for trace CGA detection with a detection limit of 7.8 nM and a wide linear range of 0.5 μM to 4 mM. The exceptional sensitivity and selectivity of the sensor made it accomplish the measurements of chlorogenic acid in soft drinks and coffee with high consistency of HPLC results. The satisfactory performance of the obtained sensor enables it to be used for quality control and study of drug metabolism in PD treatments.

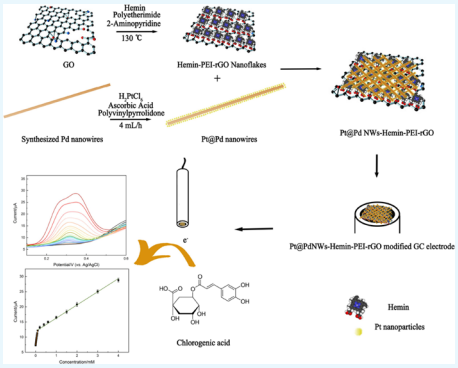

1. INTRODUCTION

Chlorogenic acid (CGA) is a phenolic compound with low toxicity and fewer side effects, which is rich in coffee, a variety of fruits, and vegetables.[1] In particular, it is also the main active ingredient in many traditional Chinese medicines, including honeysuckle and *Eucommia ulmoides*.[2] Studies show that chlorogenic acid has a variety of beneficial medicinal effects, such as antioxidant, anti-inflammatory, nerve damage protection, and anticancer activities.[3] Especially, chlorogenic acid also plays a notably important role in the prevention and treatment of periodontal disease (PD). CGA can enhance the human dental pulp stem cells' (hDPSC) development into osteoblasts by regulating Wnt signaling, which has an exceptional therapeutic prospect for patients with PD.[4] In addition, CGA is also a potential agent against periodontitis caused by microbes due to its antimicrobial activity.[5] Drug-loaded dental implants with CGA are also employed as an effective treatment to decrease the possibility of infections.[6] Therefore, accurate quantitative analysis of CGA is of great significance for PD intervention and treatment.

As a natural substance, it is hard to separate and assess CGA in a complicated system, which sets a rigorous requirement for the analytic approaches of CGA. Traditional detection methods including ultrahigh-performance liquid chromatography (UHPLC), near-infrared spectroscopy (NIRS), liquid chromatography-mass spectrometry (LC−MS), and capillary electrophoresis have been used for the determination of CGA.[7] However, these methods are usually very expensive, time-consuming, require many reagent solutions, and have low sensitivity, which makes them have intrinsic limitations in exploring further application of chlorogenic acid. Compared to the existing techniques, the simplicity of electrochemical sensors favors them to be applied in cases that require sophisticated operators with speedy procedures.[8] Detection in complicated environments can be accurately accomplished due to the outstanding specificity of the electrochemical sensors.[9] It is worth noting that the selectivity of sensors makes them suitable for carrying out a trace CGA test.[10] Therefore, to facilitate the exploration of chlorogenic acid in oral health care, facile and ultrasensitive sensors with high selectivity to detect CGA are in a huge demand.

Received: November 23, 2021
Accepted: January 21, 2022
Published: January 31, 2022

Scheme 1. Schematic Representation of the Pt@Pd NWs-Hemin-PEI-rGO Nanohybrid-Based Electrochemical Non-Enzyme Sensor

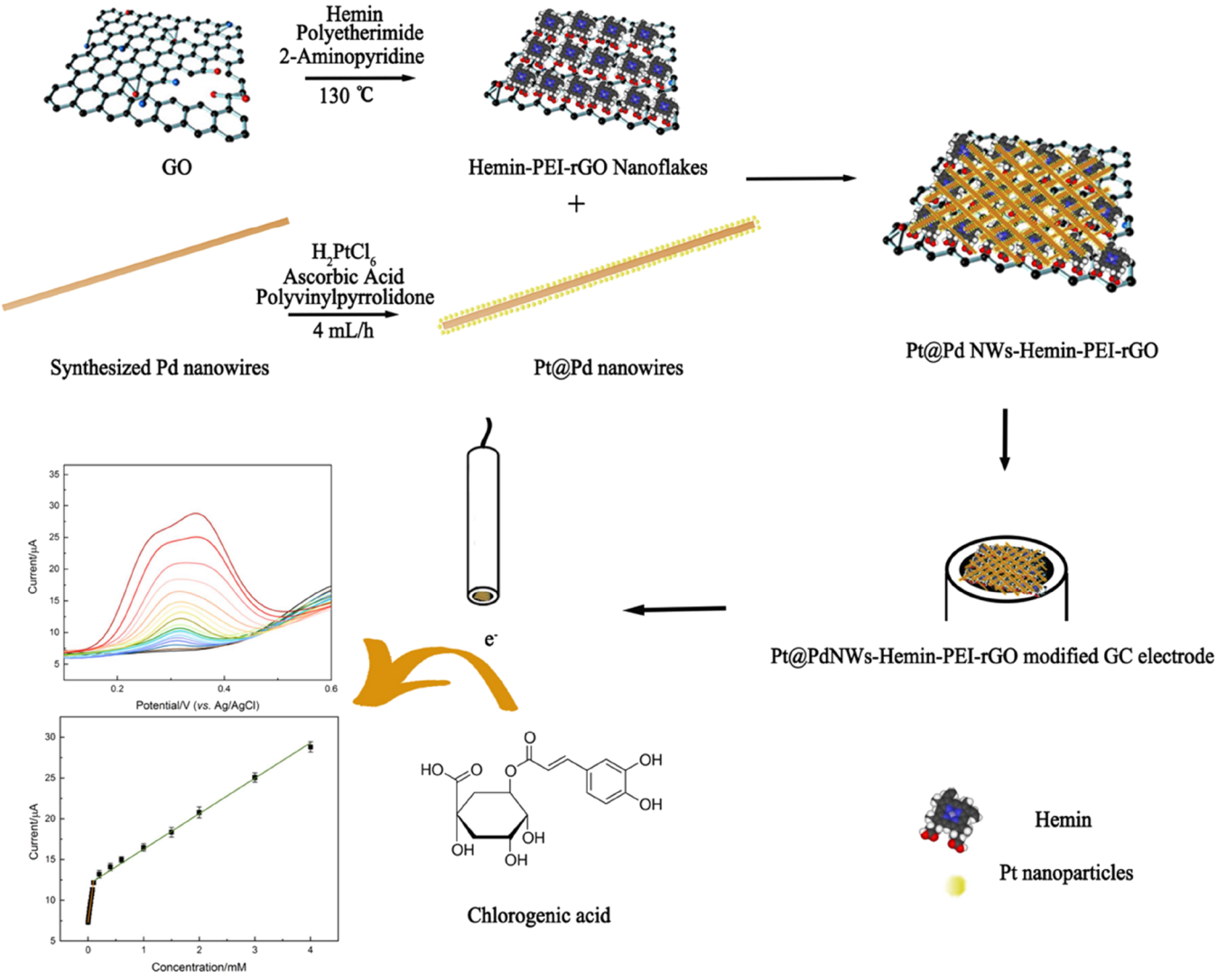

Compared with nanoparticles, one-dimensional nanostructures such as nanowires (NWs) have attracted more and more attention in the field of biosensors because of their excellent stability, high electrocatalytic activity, and enhanced conductivity.[11] The analytical performance of sensing surfaces modified with nanowires has been significantly improved.[12] Metal nanowires with a high specific surface area can not only fix more biomolecules but also have more electrocatalytic sites, which can trigger electrochemical reactions faster. Moreover, nanowires also can improve the electron transport pathway's efficiency. In addition, nanowires with a high aspect ratio can weave a tight network on the electrode, not only providing sufficient positions to load more biological molecules but also making them more stable. The interconnected nanowires can further improve the conductivity and electrocatalytic activities.[13] Hemin is a natural porphyrin iron that is able to catalyze redox reactions.[14] It forms an electron conjugated system through a π bond and valence change of iron ions with attractive redox characteristics. It can replace a series of enzymes as catalysts to enhance the response signal on the electrode surface so as to boost stronger analytical performance.[15] However, the catalytic activity of hemin is nevertheless limited by its susceptibility to oxidative self-destruction.[16] As a result, support materials with a substantial surface area are required to ensure the stability and catalytic activity of hemin. With good electrical conductivity, a large surface area, and ease of functionalization, reduced graphene oxide (rGO) has a six-membered ring structure that can bond with the porphyrin ring of hemin through π-bonds, making it an ideal material to support hemin.[17] However, reduced graphene oxide is equally prone to irreversible stacking, which still needs to be solved by certain strategies.

In this work, hemin-functionalized polyetherimide-capped rGO nanoflakes were used as a matrix loaded with platinum-nanoparticle-encapsulated palladium nanowires to form Pt@Pd NWs-Hemin-PEI-rGO nanohybrids. Additionally, controllable linear nanostructures have been synthesized by regulating the concentration of sodium iodide during the synthesis of Pd nanowires. A non-enzymatic sensor based on Pt@Pd NWs-Hemin-PEI-rGO exhibited distinguished detection performance for the quantitative analysis of chlorogenic acid (Scheme 1). Polyethylenimine (PEI) with large amounts of amino groups effectively intensified the dispersity of reduced graphene oxide, which ensured hemin to avoid self-destruction

https://doi.org/10.1021/acsomega.1c06612
ACS Omega 2022, 7, 4614−4623

and provided abundant binding sites for Pt@Pd NWs. The interwoven network structure of Pt@Pd nanowires and hemin endowed the Pt@Pd NWs-Hemin-PEI-rGO nanohybrids with high electrochemical activity toward chlorogenic acid. The obtained electrochemical sensor exhibited not only high sensitivity for the detection of chlorogenic acid with a detection limit of 7.8 nM and a wide linear range of 0.5 μM to 4 mM but also an excellent anti-interference ability and long-term stability. In the real-sample detection, the proposed sensor also showed admirable accuracy, indicating a broad application value in practical application. It is a promising competitor for quality control and analysis of metabolism to investigate the beneficial impacts of chlorogenic acid as a functional ingredient to combat periodontal disease.

2. RESULTS AND DISCUSSION

2.1. Characterization of Pt@Pd NWs-Hemin-PEI-rGO Nanohybrids. The morphological properties of the obtained materials were revealed in transmission electron microscopy (TEM) micrographs (Figure 1). As shown in Figure 1A,

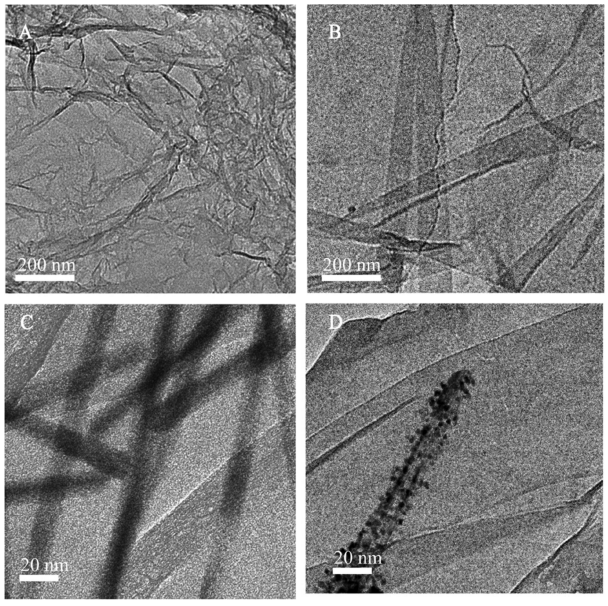

Figure 1. TEM images of (A) reduced graphene oxide (rGO), (B) Hemin-PEI-rGO nanoflakes, (C) Pd NWs-Hemin-PEI-rGO, and (D) Pt@Pd NWs-Hemin-PEI-rGO.

typically, fold characteristics with a rough surface and sheet stacking were observed on the reduced graphene oxide (rGO) flakes. After functionalization with hemin and PEI, Hemin-PEI-rGO nanoflakes displayed more extended and smooth lamellar structures than rGO, proving that the introduction of hemin did not aggravate the irreversible aggregation of rGO, while PEI effectively enhanced the dispersion. Figure 1C,D shows the TEM images of Pd NWs-Hemin-PEI-rGO and Pt@Pd NWs-Hemin-PEI-rGO nanocomposites. The Pd nanowires were strewed at random on the Hemin-PEI-rGO nanoflakes with an average diameter of 6.5 nm (Figure 1C). In Figure 1D, with nanowires as the carrying substrate, circular particles arranged on the surface and completely wrapped the nanowires. To further verify the elemental composition of the obtained nanocomposites, element analysis was carried out by energy-dispersive X-ray (EDX) spectroscopy (Figure S1). The prepared nanocomposites were composed of C, O, Fe, Pt, and Pd elements, and Cu and Si elements were from the supporting copper mesh. The existence of Fe indicated that hemin was successfully introduced into the nanohybrids.

To further verify the successful synthesis of Pt@Pd nanowires, TEM and elemental mapping were utilized to determine the structure and elemental distribution of the obtained nanohybrids. As shown in Figure S2, it can be clear that Pd was mainly concentrated in the interior of the obtained Pt@Pd, whereas Pt was deposited at the outer edge of Pt@Pd to form a dense coating structure.

The results of elemental composition analysis further declared that the obtained Pt@Pd nanowires were in double-layered structures consisting of a Pd core and a Pt outer shell (Figure 2). Figure S3 shows the X-ray diffraction spectrum of the obtained nanocomposites. A sharp diffraction peak at 2θ = 11.28° appeared in the diffraction spectrum of GO (curve a). In contrast, Hemin-PEI-rGO(b) displayed only a wider diffraction peak at 2θ = 24.3°, reflecting that the GO was reduced completely. In addition, Pd NWs-Hemin-PEI-rGO (curve c) exhibited four different diffraction peaks at 40.18, 46.56, 68.28, and 82.4°, referring to the crystal faces of (111), (200), (220), and (311), respectively, which are ascribed to the formation of the Pd NWs-Hemin-PEI-rGO nanocomposites.[18] As for the Pt@Pd NWs-Hemin-PEI-rGO (curve d), other diffraction patterns are broader owing to the superposition of lattice planes, suggesting the formation of a bimetallic nanoalloy.[19]

Diethylene glycol and ascorbic acid act as reducing agents during the synthesis of nanowires, while the concentration of iodide will affect the reduction kinetics, which has a crucial impact on the morphology of the nanowires.[20] Therefore, to ensure the consistency of a Pd NW core, the influence of sodium iodide on the nanowire synthesis has been explored in this work. Under the same experimental conditions, the amount of NaI was adjusted to be 50, 100, 150, and 200 mg, respectively. As shown in Figure 3A, the as-prepared nanomaterials showed irregular morphologies with the presence of rods, granules of various sizes, and a few cubes at the addition of 50 mg of NaI. When the addition of NaI increased to 100 mg, the nanostructures tended to have uniform cubic morphologies but varied in size, and some nanoparticles were also triangular (Figure 3B). With 150 mg of NaI, the Pd nanomaterials exhibited regular threads with uniform diameters, and no other morphological nanostructures existed. However, when the addition of NaI was further increased to 200 mg, the morphological structures of Pd nanomaterials exhibited further alterations, showing cubic and triangular structures in addition to small amounts of wire-like nanostructures. According to the above results, the subsequent synthesis procedures for nanomaterials in order to construct sensing surfaces all adopted the protocol of 150 mg NaI.

2.2. Electrochemical Characterization. To investigate the electrochemical property of stepwise-modified electrodes, cyclic voltammetry (CV) analysis in a KCl (100 mM) aqueous solution containing 10 mM $[Fe(CN)_6]^{3-/4-}$ as a redox probe has been utilized. As shown in Figure 4A, compared with the bare glassy carbon electrode (GCE) (yellow), the peak current of Pt@Pd NWs-Hemin-PEI-rGO/GCE was significantly higher, indicating that the sensing surface modified with Pt@Pd NWs-Hemin-PEI-rGO exhibited an excellent electrical conductivity and had the potential to achieve more sensitive detection. Under the same conditions, the values of peak current were ranked as follows: Pt@Pd NWs-Hemin-PEI-

https://doi.org/10.1021/acsomega.1c06612
ACS Omega 2022, 7, 4614−4623

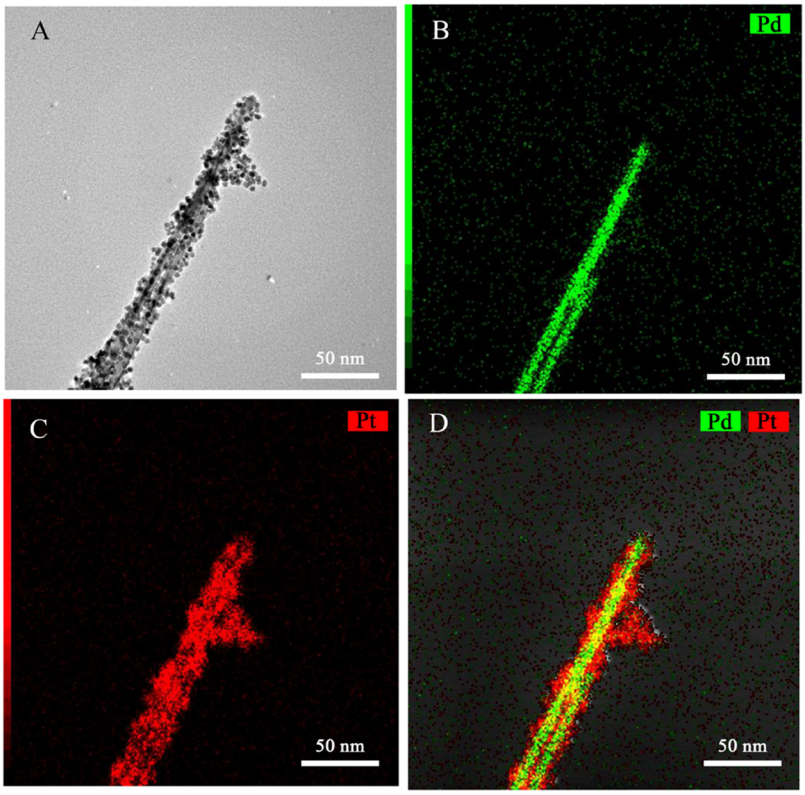

Figure 2. Elemental composition analysis of Pt@Pd NWs. (A) TEM image of a Pt@Pd nanowire; (B–D) the elemental mapping images of a Pt@Pd nanowire: Pd, Pt, and overlay of Pt and Pd.

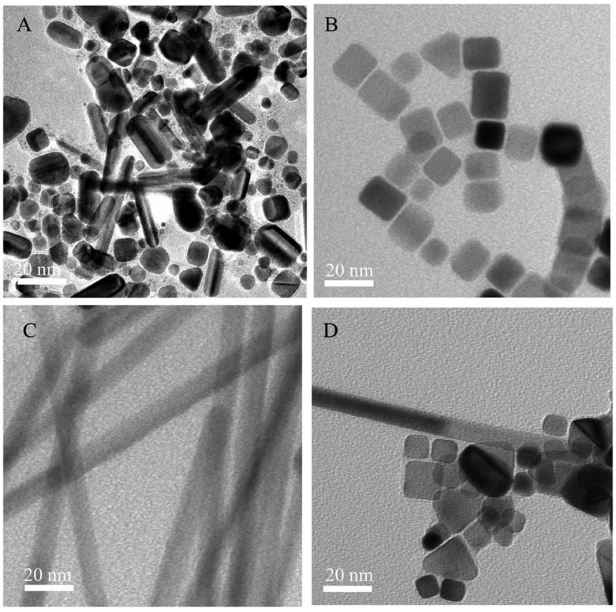

Figure 3. TEM images of Pd nanostructures synthesized under the same condition with the addition of different amounts of NaI: (A) 50, (B) 100, (C) 150, and (D) 200 mg.

rGO/GCE > Pd NWs-Hemin-PEI-rGO/GCE > Hemin-PEI-rGO/GCE > bare GCE. In addition, the electroactive surface area of different GCEs has been evaluated by the Randles–Sevcik equation:[21]

$$I_p = 2.69 \times 10^5 \times A_{eff} \times D^{1/2} \times n^{3/2} \times v^{1/2} \times c \quad (1)$$

where I_p is the redox peak current, A_{eff} corresponds to the electroactive surface area (A_{eff}, cm^2), the diffusion coefficient (D) of the redox probe is $(6.70 \pm 0.02) \times 10^{-6}$ cm^{-2}/s, n represents the number of transferred electrons involved in the redox reaction, and V is the applied scan rate. The Pt@Pd NWs-Hemin-PEI-rGO/GCE exhibited the largest effective electroactive area of 0.079 cm^2, which was 1.27-, 1.47-, and 1.59-fold larger than Pd NWs-Hemin-PEI-rGO/GCE, Hemin-PEI-rGO/GCE, and bare GCE, respectively. This result further demonstrated the ability of Pt@Pd NWs-Hemin-PEI-rGO in increasing the electrical conductivity as well as enhancing the electroactive surface area. Meanwhile, electron transfer can be investigated by contrasting the peak separation (ΔE_p). It can be observed that with the stepwise modification of nanomaterials, the ΔE_p between the redox peaks also decreased in a stepwise manner. After the modification of Pt@Pd NWs-Hemin-PEI-rGO, ΔE_p declined from 147 mV (bare electrode) to 110 mV, revealing that the Pt@Pd NWs-Hemin-PEI-rGO/GCE had a faster electron transfer rate, which facilitated electron transports between the electrolyte and electrode. The above phenomenon can be attributed to the possession of a larger effective electroactive area by Hemin-PEI-rGO nanoflakes, which provides more sites for the loading of Pt@Pd NWs with high conductivity. Meanwhile, the net structure formed by Pt@Pd NWs also contributes to further improve the electrical conductivity of the hybrid composites.

The CV curves of CGA at different nanomaterial-modified electrodes recorded at a scan rate of 50 mV/s in the presence and absence of chlorogenic acid are shown in Figure 4B. It is found that no observable redox peaks existed on the Pt@Pd NWs-Hemin-PEI-rGO/GCE in the absence of chlorogenic acid, while a prominent redox peak appeared at 0.26 V/0.2 V

https://doi.org/10.1021/acsomega.1c06612
ACS Omega 2022, 7, 4614–4623

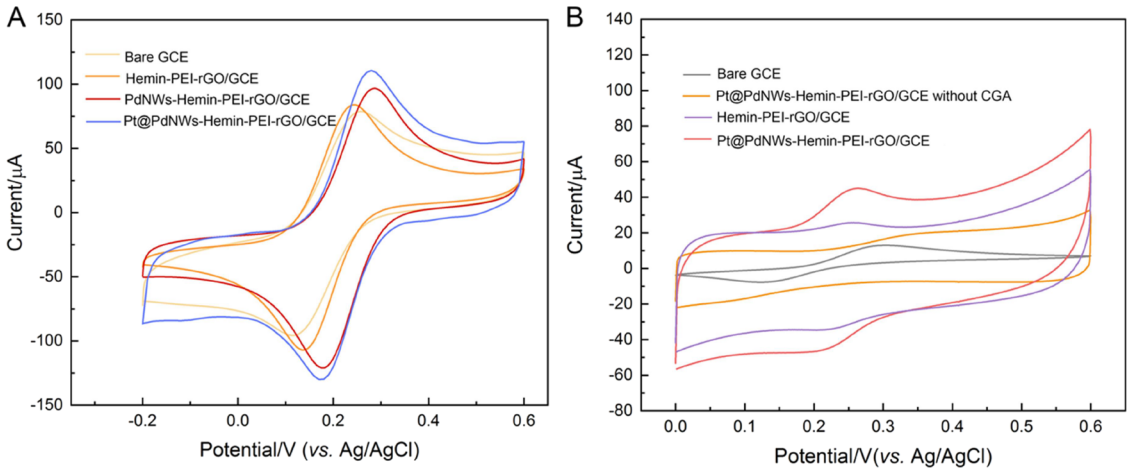

Figure 4. (A) Electrochemical behavior analysis of electrodes modified with different nanomaterials: bare GCE (yellow), Hemin-PEI-rGO/GCE (orange), Pd NWs-Hemin-PEI-rGO/GCE (red), and Pt@Pd NWs-Hemin-PEI-rGO/GCE (blue) (10 mM $[Fe(CN)_6]^{3-/4-}$ containing 0.1 M KCl); (B) CV profiles of the bare GCE (gray), Hemin-PEI-rGO/GCE with CGA (purple), and Pt@Pd NWs-Hemin-PEI-rGO/GCE with CGA (0.5 mM) (red) and without CGA (orange) in 0.1 M PBS (pH 4) at a scan rate of 50 mV s^{-1}.

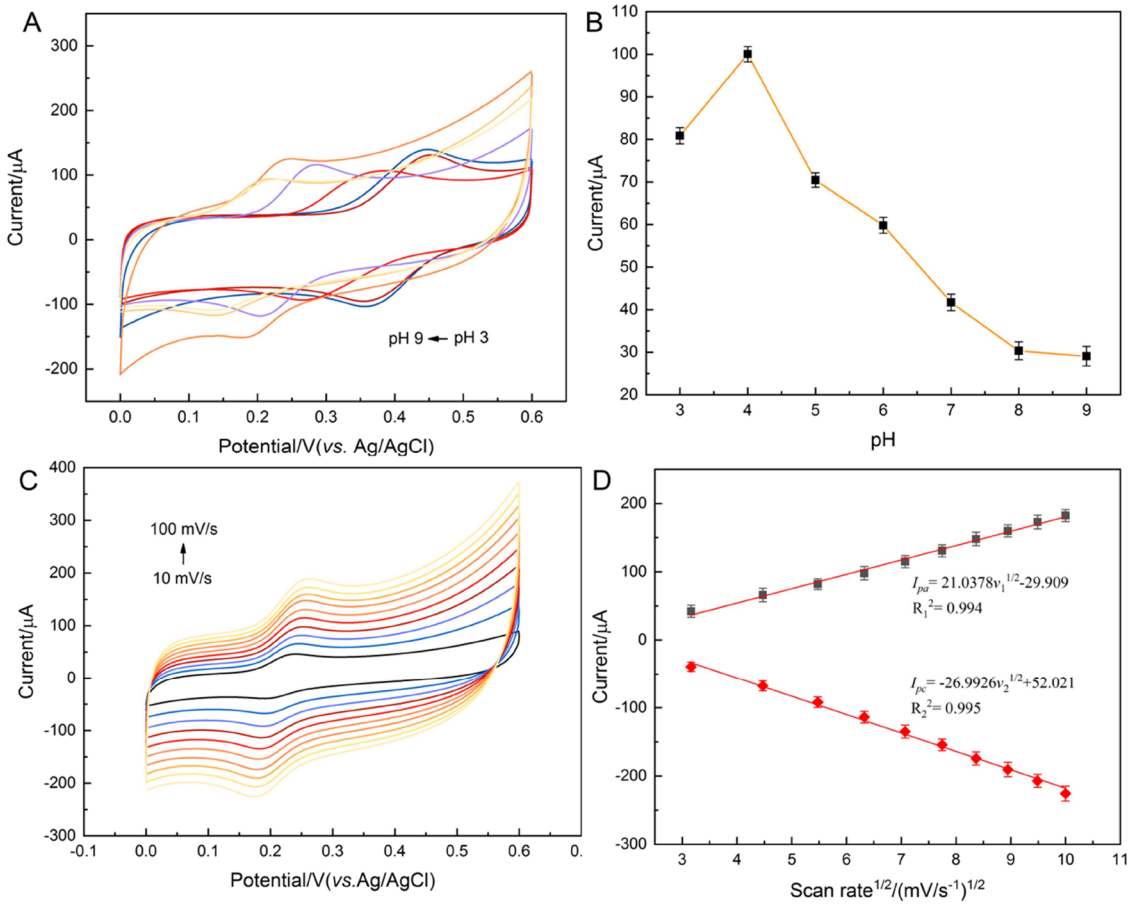

Figure 5. (A) CVs of Pt@Pd NWs-Hemin-PEI-rGO/GCE in PBS solution (0.1 M) with different pH values. (B) Linear relationship obtained for the peak current vs pH value (n = 5). (C) CV curves of CGA at the Pt@Pd NWs-Hemin-PEI-rGO/GCE in a pH 4 0.1 M phosphate buffer solution at various scan rates (10, 20, 30, 40, 50, 60, 70, 80, 90, and 100 mV s^{-1}). (D) Linear relationship obtained for the peak current vs square root of the scan rate (n = 5).

in the presence of chlorogenic acid. This result proved that the obtained nanohybrids owned good electrocatalytic activity toward chlorogenic acid and could be an ideal candidate for chlorogenic acid detection. Moreover, compared with the bare GCE, Hemin-PEI-rGO/GCE displayed weak redox peaks, while the electrochemical response toward CGA was further enhanced due to the addition of Pt@Pd NWs. Additionally, the I_{pa}/I_{pc} value was 1.32, larger than 1, which indicated that the catalytical action of the CGA on the proposed sensing surface was a quasi-reversible process.[22] These results

https://doi.org/10.1021/acsomega.1c06612
ACS Omega 2022, 7, 4614−4623

demonstrate that hemin exhibits a certain electrocatalytic activity toward chlorogenic acid, and the addition of NWs greatly increases the redox signal of CGA, which makes the obtained Pt@Pd NWs-Hemin-PEI-rGO nanohybrids have higher electrochemical reactivity toward the redox of chlorogenic acid. Therefore, the GCE modified with Pt@Pd NWs-Hemin-PEI-rGO shows a remarkable performance on the CGA analysis, which has a great potential for trace detection of chlorogenic acid.

2.3. Optimization of the Experimental Variables. The electrochemical behaviors of CGA on the Pt@Pd NWs-Hemin-PEI-rGO/GCE in 0.1 M phosphate buffer with varying pH values were studied using cyclic voltammetry (CV). As shown in Figure 5A, a pair of redox peaks can be observed, and the peak potential shifted to a more negative direction with increasing pH. Furthermore, it can be found that the electrochemical activity of Pt@Pd NWs-Hemin-PEI-rGO/GCE depends on the pH value of the buffer. The peak current of the oxidation reaction gradually enhanced as the pH value increased from 3 to 4 and then decreased step by step as pH further increased to 9. The as-prepared electrode showed significantly higher electrochemical activity at a pH value of 4 and a stronger response signal of chlorogenic acid. Therefore, PBS buffer with a pH value of 4 was used as the supporting solution for subsequent experiments.

Figure 5C records the cyclic voltammetric curves of the Pt@Pd NWs-Hemin-PEI-rGO/GCE at different scan rates in PBS electrolyte solution containing 0.5 mM chlorogenic acid at pH 4. The cathodic and anodic peak currents showed a good linear relationship with the square root of the scan rate from 10 to 100 mV/s (Figure 5D). The linear regression equations can be expressed as $I_{pa} = 21.0378v^{1/2} - 29.909$ ($R^2 = 0.994$) and $I_{pc} = -26.9926v^{1/2} + 52.021$ ($R^2 = 0.995$), suggesting that the overall reaction kinetics are diffusion-controlled processes.[23] To ensure the stability of subsequent experiments, 50 mV/s was finally selected as the scan rate for the quantitative analysis of CGA.

2.4. Quantitative Performance of the Pt@Pd NWs-Hemin-PEI-rGO/GCE. To evaluate the analytical capability of the Pt@Pd NWs-Hemin-PEI-rGO/GCE, different concentrations of chlorogenic acid were selected as the target analytes, which were determined by the differential pulse voltammetry method (DPV). Under the optimal experimental conditions, the DPV curves of different concentrations of CGA are recorded in Figure 6A. It can be obviously observed that with the increased CGA concentration, the electrochemical response at the electrode surface linearly enhanced, indicating that the proposed sensor was sufficient and sensitive for the determination of CGA. We fitted the calibration curve after five independent tests. There was an obvious linear relationship between the peak current and the concentration of CGA (Figure 6B). From the calibrated current−concentration profile, the obtained sensor showed two linear ranges from 0.5 μM to 0.1 mM and from 0.1 to 4 mM with regression coefficient (R^2) values of 0.994 and 0.993, respectively. The linear regression equations can be expressed as follows:

$$I_1 = 51.4698C + 7.2934 \quad (2)$$

where the range is from 0.5 μM to 0.1 mM, $R^2 = 0.994$.

$$I_2 = 4.3484C + 11.9282 \quad (3)$$

where the range is from 0.1 to 4 mM, $R^2 = 0.993$.

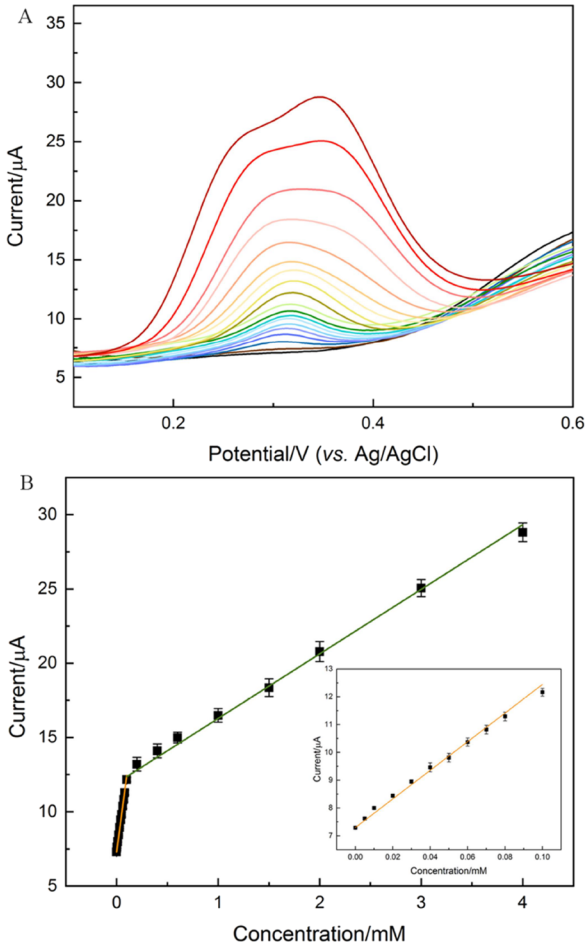

Figure 6. (A) Differential pulse voltammetry (DPV) curves of the Pt@Pd NWs-Hemin-PEI-rGO/GCE in PBS buffer solution (pH 4) containing various concentrations of CGA. (B) Corresponding calibration curve of the response current versus the concentration of CGA. Inset is the linear relationship between the current response and the low concentration of CGA ($n = 5$).

A detection limit of 7.8 nM and sensitivity of 651.523 μA μM^{-1} cm^{-2} were obtained according to the LOD = 3Sb/s at a signal-to-noise ratio of 3. The superior electrochemical performance of the Pt@Pd NWs-Hemin-PEI-rGO/GCE was attributed to the remarkable electroactive area of the Hemin-PEI-rGO nanoflakes, which significantly accelerated the electron transport efficiently during the detection process. Meanwhile, hemin and Pt@Pd NWs both exhibited electrocatalytic activity toward chlorogenic acid, which had synergistic effects on enhancing the signal response on the sensing interface. Therefore, the Pt@Pd NWs-Hemin-PEI-rGO-modified sensing surface possessed excellent trace analysis ability for CGA.

A comparison of the performances of traditional detection methods and the reported sensor for the detection of chlorogenic acid is completed in Table1. It can be clearly seen that the constructed novel chlorogenic acid detection platform has a relatively low detection limit, and the detection linear range is also significantly broadened. The proposed sensor based on Pt@Pd NWs-Hemin-PEI-rGO nanohybrids owns an admirable analytical performance for CGA, which makes it a powerful tool for further research on the mechanism of CGA in oral health care. It also has the potential to be a

https://doi.org/10.1021/acsomega.1c06612
ACS Omega 2022, 7, 4614−4623

Table 1. Comparisons of Analytical Parameters for Detection of CGA among Previously Described Methods and the Obtained Sensor in this Work

materials	detection range	LOD	ref
HPLC	4.56−47.2 μmol L^{-1}	3.78 μmol L^{-1}	24
UHPLC−MS	28.2−1552.4 μmol L^{-1}	11.79 μmol L^{-1}	25
electrochemistry & UV−vis absorption spectroscopy	0.5−60 μmol L^{-1}	45 nmol L^{-1}	26
water-compatible magnetic molecularly imprinted polymers	0.14−564.5 μmol L^{-1}	28 nmol L^{-1}	27
C-SPE/Pt-NPs/RGO/lacc-biosensor	2.91−24.67 μmol L^{-1}	2.67 μmol L^{-1}	28
mesoporous carbon−ionic liquid paste electrode	2.5 μmol L^{-1}−20 nmol L^{-1}	10 nmol L^{-1}	29
Pt@Pd NWs-Hemin-PEI-rGO/GCE	0.5 μmol L^{-1}−4 mmol L^{-1}	7.8 nmol L^{-1}	this work

quality monitoring platform in the development of daily nutrients against periodontitis.

2.5. Stability, Repeatability, and Interference Immunity Studies. To ensure the accuracy and stability of the Pt@Pd NWs-Hemin-PEI-rGO/GCE in real detection, a series of important parameters of the sensor had been examined. First, the stability of the sensing surface was determined by regular detection of its current response. The proposed GCE was stored in a refrigerator at 4 °C for 1 month and tested every 5 days in 0.1 M PBS solution containing 0.5 mM chlorogenic acid. After storage for 30 days, the peak current response of the GCE still maintained 95.7% of the original current with acceptable stability. The reproducibility of the obtained GCE in the analysis of chlorogenic acid was verified by five independent experiments, and the results are shown in Figure S4. The DPV response signals of five independent groups did not show obvious inconsistency with an RSD of 2.18%, indicating an exceptional reproducibility of the proposed sensor. As for the specificity of the prepared sensor, an anti-interference study was carried out using a 25-fold excess of chicory acid, caffeic acid, glucose, ascorbic acid, uric acid, and catechol as interferences. In Figure S5, the variation of current caused by interfering substances was less than 5% compared with the current response of the unperturbed GCE, illustrating that the Pt@Pd NWs-Hemin-PEI-rGO/GCE acquired favorable selectivity and specificity.

2.6. Application in Real Samples. To assess the utility of the Pt@Pd NWs-Hemin-PEI-rGO/GCE, the concentration of CGA in commercial soft drinks and coffee was determined using the standard addition method, which could overcome the matrix effects. Ten milliliters of commercial beverages and coffee were added with 25 mL of PBS buffer under stirring. Then, different concentrations of chlorogenic acid were added to the real samples sequentially. The detection was performed under the optimal condition, and five sets of parallel detections were performed for each sample. The analytical results are shown in Table 2. The Pt@Pd NWs-Hemin-PEI-rGO/GCE showed an appreciable response to the real samples with the addition of chlorogenic acid with excellent recoveries from 97.72 to 102.13%. The result evinces that the sensor based on Pt@Pd NWs-Hemin-PEI-rGO has a great potential in real-sample analysis, which opens a road for drug development based on chlorogenic acid to guarantee oral health.

Table 2. Determination of CGA in Various Real Samples by the Pt@Pd NWs-Hemin-PEI-RGO/GCE

sample	added (μM)	found (μM)	recovery (%)	RSD
soft drink	25	25.54	102.13	2.87
	50	50.1	100.21	2.72
	100	99.84	99.85	2.08
	150	152.26	101.51	2.17
coffee	25	25.26	101.3	2.87
	50	48.87	97.72	2.46
	100	100.19	100.21	2.09
	150	148.33	99.89	2.43

3. CONCLUSIONS

In this work, an ultrasensitive electrochemical sensor for the determination of CGA based on Pt@Pd NWs-Hemin-PEI-rGO nanohybrids has been developed. The impacts of NaI on the formation of a nanostructure in the preparation of Pd nanowires have also been discussed, and a method to obtain Pd nanowires with excellent morphology has been determined. Subsequently, Pt nanoparticles were successfully attached to palladium nanowires to form bimetallic core−shell nanowires. Along with the Hemin-PEI-rGO nanoflakes as the substrate, Pt@Pd NWs-Hemin-PEI-rGO nanohybrids with high electrochemical properties have been proposed. The hybrid nanomaterial exhibited excellent electrochemical activity, which could effectively increase the electron transfer rate and electroactive area. In addition, Pt@Pd NWs-Hemin-PEI-rGO nanohybrids exhibited admirable electrocatalytic ability for chlorogenic acid as well, facilitating the sensitive detection of CGA. The obtained sensor has a detection limit up to the nanometer scale and a linear range from 0.5 μM to 4 mM with excellent analytical capabilities beyond traditional detection methods and reported CGA sensors. In real-sample detection, it also exhibited satisfactory performance, suggesting its future potential in the in-depth study of CGA in prevention of oral disease.

4. EXPERIMENTAL SECTION

4.1. Chemicals and Reagents. Graphene oxide was obtained from Nanjing XFNANO Materials Tech Co. (Nanjing, China). Polyethyleneimine, hemin, 2-aminopyridine, ethanol, polyvinylpyrrolidone (MW = 58000), ascorbic acid, sodium iodide, sodium tetrachloropalladate, diethylene glycol, potassium bromide, chloroplatinic acid hydrate, chlorogenic acid, ethylene glycol, caffeic acid, catechol, and glucose were fully acquired from Sigma-Aldrich Co. (St. Louis, MO, USA). All the chemicals were analytically pure and used as received without further purification. Deionized water was used throughout the experiments unless otherwise indicated.

4.2. Apparatus and Measurements. A high-pressure reactor (JULABO BR-25/40) was used for nanomaterial synthesis. Transmission electron microscopy (TEM) was performed by a JEM 2100 (Japan Electron Optics Laboratory). With a typical three-electrode system, cyclic voltammetry (CV), and differential pulse voltammetry (DPV) were carried out by using an electrochemical analyzer (CHI 760E, China) with software. The electrochemical behavior of glassy carbon electrodes modified by different nanomaterials was analyzed by a traditional three-electrode system. The working electrode was modified by different nanomaterials, and Ag/AgCl and Pt wires with saturated KCl solution as electrolyte were used as a reference electrode and counter electrode, respectively. All

https://doi.org/10.1021/acsomega.1c06612
ACS Omega 2022, 7, 4614−4623

electrochemical tests were performed at room temperature. Under the electrochemical test system, the electrochemical properties of the developed electrode were investigated by differential pulse voltammetry (DPV) and cyclic voltammetry (CV). In the standard experiment, the electrolyte support solutions were 10 mM $[Fe(CN)_6]^{3-/4-}$ with 0.1 M KCl solution as a redox probe and 0.1 M PBS buffer with pH 4.

4.3. Preparation of Hemin-PEI-rGO Nanoflakes. Hemin-PEI-RGO nanoflakes were prepared by a one-step hydrothermal method. First, polyethyleneimine (PEI) was added to 50 mL of 1 mg/mL GO solution in a ratio of 1:10 with sonication at room temperature for 2 h to obtain a uniform PEI-GO aqueous solution. Subsequently, 5 mg of hemin and 5 g of 2-aminopyridine were added to 50 mL of PEI-GO solution under magnetic stirring. After 20 min of stirring, the mixture was transferred to a Teflon-lined autoclave and reacted at 130 °C for 3 h. Finally, a black precipitate was obtained by continuously washing with ultrapure water and absolute ethanol three times. The solid product Hemin-PEI-rGO with a flaky shape was obtained by vacuum drying.

4.4. Preparation of Pt@Pd Nanowires. One hundred five milligrams of PVP, 100 mg of AA, and 150 mg of NaI were dissolved in 10 mL of DEG and preheated in an oil bath at 160 °C for 15 min with stirring. Then, 3 mL of DEG solution containing 50 mg of Na_2PdCl_4 was added drop by drop. After the reaction for 2 h, the reaction was terminated on ice. Finally, the product, namely, Pd nanowires, was collected by centrifugation, washed with ethanol three times, and resuspended in ultrapure water.

Two milliliters of Pd nanowire solution, 100 mg of AA, 100 mg of PVP, and 80 mg of potassium bromide solid were mixed in a three-neck flask containing 13 mL of ethylene glycol and stirred at 110 °C for 15 min under magnetic stirring. Subsequently, the reaction temperature was rapidly raised to 200 °C within 30 min. At the same time, 2 mg of sodium chloroplatinate was dissolved in 15 mL of ethylene glycol, and the solution was injected into the three-neck flask at a rate of 4 mL/h using a syringe pump. After injection, the projection mixture was maintained at 200 °C for 20 min. To quench the reaction, the flask was placed on ice. The final product was collected by centrifugation and washed with ethanol three times. Finally, the obtained Pt@Pd NWs were dispersed in ultrapure water for further use.

4.5. Preparation of the Modified Sensing Electrodes. In advance, the glassy carbon electrode was polished and pretreated with alumina slurry powders in different sizes (0.05 and 0.1 μm). After obtaining the mirror-like surface, the GCE was washed with ethanol and ultrapure water under ultrasonication followed by drying with a nitrogen stream. Six microliters of Hemin-PEI-rGO solution was applied dropwise on the surface of the glassy carbon electrode. After drying in a 40 °C vacuum oven, a black film was obtained on the surface of the GCE. Then, a 6 μL Pt@Pd NWs suspension was modified on the Hemin-PEI-rGO/GCE by dip-coating and dried in a vacuum oven. As an experimental control group, rGO, Hemin-PEI-rGO/GCE, and Pd NWs/Hemin-PEI-rGO/GCE were prepared similarly.

■ ASSOCIATED CONTENT

Supporting Information

The Supporting Information is available free of charge at https://pubs.acs.org/doi/10.1021/acsomega.1c06612.

(Figure S1) Energy-dispersive X-ray spectroscopy (EDX) spectrum of Pt@Pd NWs-Hemin-PEI-rGO nanocomposites, (Figure S2) TEM images of Pt@Pd NWs, (Figure S3) XRD patterns of different nanomaterials (Figure S4) the column graph of DPV signals in PBS buffer solution (pH 4) containing 0.5 mM of CGA at five different electrodes prepared under the same conditions, (Figure S5) the current response of interfering substances 25-fold alone and compounds of interfering substances and CGA (n = 5) (PDF)

■ AUTHOR INFORMATION

Corresponding Author

Jian Jiao − *Department of Stomatology, Tianjin Medical University General Hospital, Tianjin 300052, China; School of Dentistry, Stomatological Hospital, Tianjin Medical University, Tianjin 300070, China;* orcid.org/0000-0001-6002-7297; Email: Jiaojian1985@tmu.edu.cn

Authors

Wei Li − *Department of Stomatology, Tianjin Medical University General Hospital, Tianjin 300052, China*

Xiuli Deng − *Department of Stomatology, Tianjin Medical University General Hospital, Tianjin 300052, China; Tianjin Beichen Traditional Chinese Medicine Hospital, Tianjin 300400, China*

Ziyu Wu − *Tianjin Beichen Traditional Chinese Medicine Hospital, Tianjin 300400, China*

Louqiang Zhang − *Department of Stomatology, Tianjin Medical University General Hospital, Tianjin 300052, China*

Complete contact information is available at: https://pubs.acs.org/10.1021/acsomega.1c06612

Author Contributions

Conceptualization, data curation, investigation, and writing of the original draft were performed by W.L. and X.D.; formal analysis was done by L.Z.; methodology was established by W.L. and Z.W.; project administration and reviewing and editing the paper were performed by J.J. All authors have read and agreed to the published version of the manuscript.

Notes

The authors declare no competing financial interest.

The authors declare that they have no known competing financial interests or personal relationships that could have appeared to influence the work reported in this paper.

■ ACKNOWLEDGMENTS

This work was supported by the Science and Technology Project of Tianjin Health Commission with grant no. KJ20010.

■ REFERENCES

(1) (a) Bouayed, J.; Rammal, H.; Dicko, A.; Younos, C.; Soulimani, R. Chlorogenic acid, a polyphenol from Prunus domestica (Mirabelle), with coupled anxiolytic and antioxidant effects. *J. Neurol. Sci.* **2007**, *262*, 77−84. (b) Qie, X.; Chen, W.; Zeng, M.; Wang, Z.; Chen, J.; Goff, H. D.; He, Z. Interaction between β-lactoglobulin and chlorogenic acid and its effect on antioxidant activity and thermal stability. *Food Hydrocolloids* **2021**, *121*, 107059.

(2) (a) Upadhyay, R.; Mohan Rao, L. J. An outlook on chlorogenic acids—occurrence, chemistry, technology, and biological activities. *Crit. Rev. Food Sci. Nutr.* **2013**, *53*, 968−984. (b) Xu, W.; Zhang, X.; Wang, L.; Zeng, W.; Sun, Y.; Zhou, C.; Zhou, T.; Shen, M. Effect of chlorogenic acid on the quorum sensing system of clinically isolated

multidrug-resistant Pseudomonas aeruginosa. *J. Appl. Microbiol.* **2022**, 1008.
(3) (a) Heitman, E.; Ingram, D. K. Cognitive and neuroprotective effects of chlorogenic acid. *Nutr. Neurosci.* **2017**, *20*, 32−39. (b) Sadeghi Ekbatan, S.; Li, X.-Q.; Ghorbani, M.; Azadi, B.; Kubow, S. Chlorogenic acid and its microbial metabolites exert anti-proliferative effects, S-phase cell-cycle arrest and apoptosis in human colon cancer caco-2 cells. *Int. J. Mol. Sci.* **2018**, *19*, 723. (c) Ali, N.; Rashid, S.; Nafees, S.; Hasan, S. K.; Shahid, A.; Majed, F.; Sultana, S. Protective effect of Chlorogenic acid against methotrexate induced oxidative stress, inflammation and apoptosis in rat liver: An experimental approach. *Chem.-Biol. Interact.* **2017**, *272*, 80−91. (d) Lu, H.; Tian, Z.; Cui, Y.; Liu, Z.; Ma, X. Chlorogenic acid: A comprehensive review of the dietary sources, processing effects, bioavailability, beneficial properties, mechanisms of action, and future directions. *Compr. Rev. Food Sci. Food Saf.* **2020**, *19*, 3130−3158.
(4) Hu, X.; Wang, L.; He, Y.; Wei, M.; Yan, H.; Zhu, H. Chlorogenic Acid Promotes Osteogenic Differentiation of Human Dental Pulp Stem Cells Through Wnt Signaling. *Stem Cells Dev.* **2021**, 641.
(5) Tsou, S.-H.; Hu, S.-W.; Yang, J.-J.; Yan, M.; Lin, Y.-Y. Potential oral health care agent from coffee against virulence factor of periodontitis. *Nutrients* **2019**, *11*, 2235.
(6) Brum, R. S.; Labes, L. G.; Volpato, C. Â. M.; Benfatti, C. A. M.; Pimenta, A. d. L. Strategies to Reduce Biofilm Formation in PEEK Materials Applied to Implant Dentistry—A Comprehensive Review. *Antibiotics* **2020**, *9*, 609.
(7) (a) Kendir, G.; Güvenç, A.; Dinç, E. Ultra-performance liquid chromatographic (UPLC) determination of the rutin and chlorogenic acid in the Ribes anatolica and its antioxidant activity. *Planta Med.* **2011**, *77*, PA36. (b) Li, Z.; Huang, D.; Tang, Z.; Deng, C.; Zhang, X. Fast determination of chlorogenic acid in tobacco residues using microwave-assisted extraction and capillary zone electrophoresis technique. *Talanta* **2010**, *82*, 1181−1185. (c) Wen, J.; Kang, L.; Liu, H.; Xiao, Y.; Zhang, X.; Chen, Y. A validated UV-HPLC method for determination of chlorogenic acid in Lepidogrammitis drymoglossoides (Baker) Ching, Polypodiaceae. *Pharm. Res.* **2012**, *4*, 148. (d) Dai, C.-y.; Gao, X.-y. B.; Fu, Y.; Liu, H.-a. Determination of the contents of chlorogenic acid and phillyrin of shuanghuanglian oral fluid using NIRS. *Spectrosc. Spectral Anal.* **2010**, *30*, 358−362.
(8) (a) Jiao, J.; Pan, M.; Liu, X.; Liu, J.; Li, B.; Chen, Q. An Ultrasensitive Non-Enzymatic Sensor for Quantitation of Anti-Cancer Substance Chicoric Acid Based on Bimetallic Nanoalloy with Polyetherimide-Capped Reduced Graphene Oxide. *Nanomaterials* **2020**, *10*, 499. (b) Wang, Z.; Wang, Y.; Yang, S.; Xue, L.; Feng, W.; Liu, X.; Li, B.; Yin, M.; Jiao, J.; Chen, Q. Electrochemical sensor based on magnetic nanohybrids of multiple phthalocyanine doped ferrites/CMWCNTs for detection of rosmarinic acid. *Talanta* **2021**, *226*, 122165. (c) Karimi-Maleh, H.; Khataee, A.; Karimi, F.; Baghayeri, M.; Fu, L.; Rouhi, J.; Karaman, C.; Karaman, O.; Boukherroub, R. A green and sensitive guanine-based DNA biosensor for idarubicin anticancer monitoring in biological samples: A simple and fast strategy for control of health quality in chemotherapy procedure confirmed by docking investigation. *Chemosphere* **2021**, *132928*, 132928. (d) Gupta, V. K.; Karimi-Maleh, H.; Sadegh, R. Simultaneous determination of hydroxylamine, phenol and sulfite in water and waste water samples using a voltammetric nanosensor. *Int. J. Electrochem. Sci.* **2015**, *10*, 303−316.
(9) Karimi-Maleh, H.; Karimi, F.; Fu, L.; Sanati, A. L.; Alizadeh, M.; Karaman, C.; Orooji, Y. Cyanazine herbicide monitoring as a hazardous substance by a DNA nanostructure biosensor. *J. Hazard. Mater.* **2022**, *423*, 127058.
(10) Karimi-Maleh, H.; Tahernejad-Javazmi, F.; Ensafi, A. A.; Moradi, R.; Mallakpour, S.; Beitollahi, H. A high sensitive biosensor based on FePt/CNTs nanocomposite/N-(4-hydroxyphenyl)-3, 5-dinitrobenzamide modified carbon paste electrode for simultaneous determination of glutathione and piroxicam. *Biosens. Bioelectron.* **2014**, *60*, 1−7.
(11) (a) Ahmad, R.; Mahmoudi, T.; Ahn, M.-S.; Hahn, Y.-B. Recent advances in nanowires-based field-effect transistors for biological sensor applications. *Biosens. Bioelectron.* **2018**, *100*, 312−325. (b) Saenchoopa, A.; Klangphukhiew, S.; Somsub, R.; Talodthaisong, C.; Patramanon, R.; Daduang, J.; Daduang, S.; Kulchat, S. A Disposable Electrochemical Biosensor Based on Screen-Printed Carbon Electrodes Modified with Silver Nanowires/HPMC/Chitosan/Urease for the Detection of Mercury (II) in Water. *Biosensors* **2021**, *11*, 351. (c) Zhang, Y.; Gao, F.; You, H.; Li, Z.; Zou, B.; Du, Y. Recent advances in one-dimensional noble-metal-based catalysts with multiple structures for efficient fuel-cell electrocatalysis. *Coord. Chem. Rev.* **2022**, *450*, 214244. (d) Gao, F.; Zhang, Y.; Song, P.; Wang, J.; Yan, B.; Sun, Q.; Li, L.; Zhu, X.; Du, Y. Shape-control of one-dimensional PtNi nanostructures as efficient electrocatalysts for alcohol electrooxidation. *Nanoscale* **2019**, *11*, 4831−4836.
(12) (a) Li, S.; Qu, L. M.; Wang, J. F.; Ran, X. Q.; Niu, X. Acetylcholinesterase based rGO-TEPA-Copper nanowires biosensor for detecting malathion. *Int. J. Electrochem. Sci.* **2020**, *15*, 505−514. (b) Li, Z.; Gao, F.; Gu, Z. Vertically aligned Pt nanowire array/Au nanoparticle hybrid structure as highly sensitive amperometric biosensors. *Sens. Actuators, B* **2017**, *243*, 1092−1101. (c) Song, D.; Li, Y.; Lu, X.; Sun, M.; Liu, H.; Yu, G.; Gao, F. Palladium-copper nanowires-based biosensor for the ultrasensitive detection of organophosphate pesticides. *Anal. Chim. Acta* **2017**, *982*, 168−175. (d) Fu, X.; Chen, Z.; Shen, S.; Xu, L.; Luo, Z. Highly sensitive nonenzymatic glucose sensor based on reduced graphene oxide/ultrasmall Pt nanowire nanocomposites. *Int. J. Electrochem. Sci.* **2018**, *13*, 4817−4826. (e) Geng, H.; Chen, X.; Sun, L.; Qiao, Y.; Song, J.; Shi, S.; Cai, Q. ZnCuInSe/Au/TiO2 sandwich nanowires-based photoelectrochemical biosensor for ultrasensitive detection of kanamycin. *Anal. Chim. Acta* **2021**, *1146*, 166−173. (f) Gao, F.; Zhang, Y.; Ren, F.; Shiraishi, Y.; Du, Y. Universal Surfactant-Free Strategy for Self-Standing 3D Tremella-Like Pd−M (M= Ag, Pb, and Au) Nanosheets for Superior Alcohols Electrocatalysis. *Adv. Funct. Mater.* **2020**, *30*, 2000255.
(13) (a) Chen, S.-S.; Shi, Y.-C.; Wang, A.-J.; Lin, X.-X.; Feng, J.-J. Free-standing Pt nanowire networks with clean surfaces: highly sensitive electrochemical detection of nitrite. *J. Electroanal. Chem.* **2017**, *791*, 131−137. (b) Ding, M.; Liu, Y.; Wang, G.; Zhao, Z.; Yin, A.; He, Q.; Huang, Y.; Duan, X. Highly sensitive chemical detection with tunable sensitivity and selectivity from ultrathin platinum nanowires. *Small* **2017**, *13*, 1602969. (c) Gao, F.; Zhang, Y.; Wu, Z.; You, H.; Du, Y. Universal strategies to multi-dimensional noble-metal-based catalysts for electrocatalysis. *Coord. Chem. Rev.* **2021**, *436*, 213825.
(14) Liang, Z.-X.; Song, H.-Y.; Liao, S.-J. Hemin: a highly effective electrocatalyst mediating the oxygen reduction reaction. *J. Phys. Chem. C* **2011**, *115*, 2604−2610.
(15) (a) Zhang, G.; Dasgupta, P. K. Hematin as a peroxidase substitute in hydrogen peroxide determinations. *Anal. Chem.* **1992**, *64*, 517−522. (b) Yang, Y.; Zhang, H.; Huang, C.; Yang, D.; Jia, N. Electrochemical non-enzyme sensor for detecting clenbuterol (CLB) based on MoS2-Au-PEI-hemin layered nanocomposites. *Biosens. Bioelectron.* **2017**, *89*, 461−467.
(16) Xue, T.; Jiang, S.; Qu, Y.; Su, Q.; Cheng, R.; Dubin, S.; Chiu, C. Y.; Kaner, R.; Huang, Y.; Duan, X. Graphene-supported hemin as a highly active biomimetic oxidation catalyst. *Angew. Chem., Int. Ed.* **2012**, *51*, 3822−3825.
(17) Guo, Y.; Deng, L.; Li, J.; Guo, S.; Wang, E.; Dong, S. Hemin−graphene hybrid nanosheets with intrinsic peroxidase-like activity for label-free colorimetric detection of single-nucleotide polymorphism. *ACS Nano* **2011**, *5*, 1282−1290.
(18) (a) Kou, J.; Varma, R. S. Beet juice utilization: Expeditious green synthesis of noble metal nanoparticles (Ag, Au, Pt, and Pd) using microwaves. *RSC Adv.* **2012**, *2*, 10283−10290. (b) Arunagiri, T.; Golden, T. D.; Chyan, O. Study of palladium metal particle deposition on the conductive diamond surface by XRD, XPS and electrochemistry. *Mater. Chem. Phys.* **2005**, *92*, 152−158.
(19) Salih, M. A.; Çaglar, A.; Kivrak, A.; Kivrak, H. Synthesis and Characterization of Carbon Nanotube Supported Pt-Au Catalyst and

https://doi.org/10.1021/acsomega.1c06612
ACS Omega 2022, 7, 4614−4623

Its Microwave Assisted N-Hexane Decomposition Measurements. *Nanosci. Nanotechnol.* **2017**, *4*, 132−134.
(20) Wang, C.; Wang, L.; Long, R.; Ma, L.; Wang, L.; Li, Z.; Xiong, Y. Anisotropic growth of palladium twinned nanostructures controlled by kinetics and their unusual activities in galvanic replacement. *J. Mater. Chem.* **2012**, *22*, 8195−8198.
(21) Baghayeri, M.; Ansari, R.; Nodehi, M.; Veisi, H. Designing and fabrication of a novel gold nanocomposite structure: application in electrochemical sensing of bisphenol A. *Int. J. Environ. Anal. Chem.* **2018**, *98*, 874−888.
(22) Onchoke, K. K.; Trevino, A. D. Electrochemical Characteristics of Benzanthrone Studied via Cyclic Voltammetry: Charge Transfer Redox Processes. *Anal. Chem. Lett.* **2019**, *9*, 128−142.
(23) Bukkitgar, S. D.; Shetti, N. P.; Kulkarni, R. M.; Halbhavi, S. B.; Wasim, M.; Mylar, M.; Durgi, P. S.; Chirmure, S. S. Electrochemical oxidation of nimesulide in aqueous acid solutions based on TiO2 nanostructure modified electrode as a sensor. *J. Electroanal. Chem.* **2016**, *778*, 103−109.
(24) Qiu, H.; Yang, L.; Dan, H. Simultaneous Determination of Chlorogenic Acid, Baicalin and Imperatorin in Biyanling Tablets by HPLC. *China Pharm.* **2018**, *29*, 1605−1608.
(25) Melo, L. V. d.; Sawaya, A. C. H. F. UHPLC−MS quantification of coumarin and chlorogenic acid in extracts of the medicinal plants known as guaco (Mikania glomerata and Mikania laevigata). *Rev. Bras. Farmacogn.* **2015**, *25*, 105−110.
(26) Yang, H.; Yang, L.; Yuan, Y.; Pan, S.; Yang, J.; Yan, J.; Zhang, H.; Sun, Q.; Hu, X. A portable synthesis of water-soluble carbon dots for highly sensitive and selective detection of chlorogenic acid based on inner filter effect. *Spectrochim. Acta, Part A* **2018**, *189*, 139−146.
(27) Zhao, Y.; Tang, Y.; He, J.; Xu, Y.; Gao, R.; Zhang, J.; Chong, T.; Wang, L.; Tang, X. Surface imprinted polymers based on amino-hyperbranched magnetic nanoparticles for selective extraction and detection of chlorogenic acid in Honeysuckle tea. *Talanta* **2018**, *181*, 271−277.
(28) Vasilescu, I.; Eremia, S. A. V.; Penu, R.; Albu, C.; Radoi, A.; Litescu, S. C.; Radu, G.-L. Disposable dual sensor array for simultaneous determination of chlorogenic acid and caffeine from coffee. *RSC Adv.* **2015**, *5*, 261−268.
(29) Mohammadi, N.; Najafi, M.; Adeh, N. B. Highly defective mesoporous carbon−ionic liquid paste electrode as sensitive voltammetric sensor for determination of chlorogenic acid in herbal extracts. *Sens. Actuators, B* **2017**, *243*, 838−846.

https://doi.org/10.1021/acsomega.1c06612
ACS Omega 2022, 7, 4614−4623